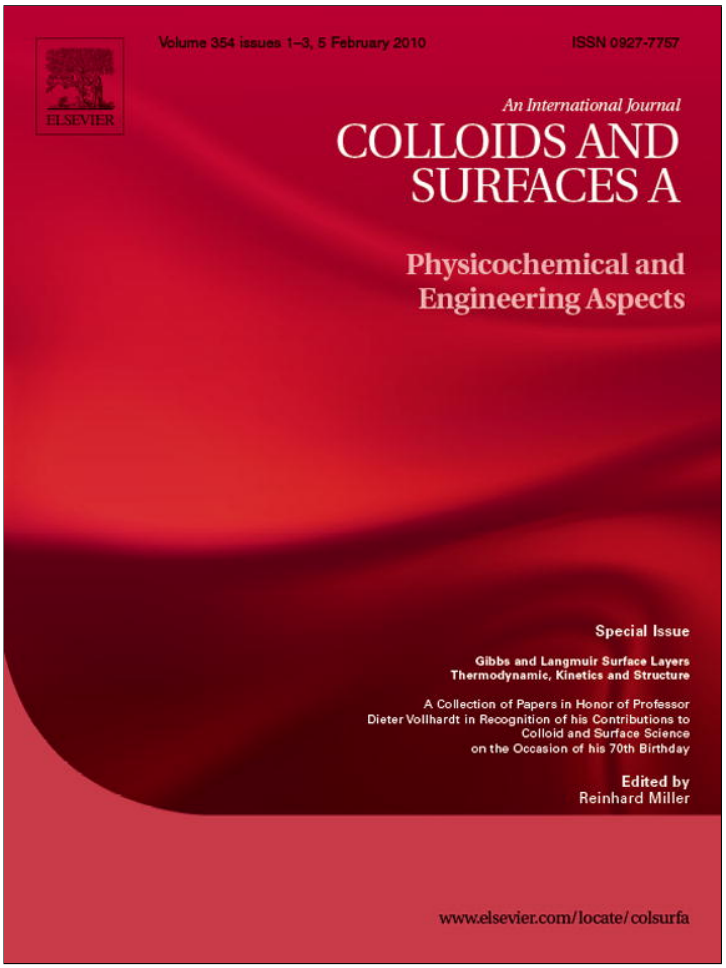

Colloids and Surfaces A: Physicochem. Eng. Aspects 354 (2010) 106–112

Contents lists available at ScienceDirect

Colloids and Surfaces A: Physicochemical and Engineering Aspects

journal homepage: www.elsevier.com/locate/colsurfa

The influence of hydrophilic spacers on the phase behavior of ether lipids

Sérgio S. Funari[a], Bernd Struth[a], Bernd Rattay[b], Gert Rapp[c], Gerald Brezesinski[d,*]

[a] HASYLAB at DESY, Notkestrasse 85, D-22607 Hamburg, Germany
[b] Institute of Pharmacy, Martin-Luther-University, Wolfgang-Langenbeck-Str. 4, 06120 Halle/S., Germany
[c] Rapp OptoElectronic, Gehenkamp 9a, D-22559 Hamburg, Germany
[d] Max Planck Institute of Colloids and Interfaces, Science Park Potsdam-Golm, Am Mühlenberg 1, D-14476 Potsdam, Germany

ARTICLE INFO

Article history:
Received 2 July 2009
Received in revised form 26 October 2009
Accepted 29 October 2009
Available online 3 November 2009

Keywords:
Phospholipids
EO-spacer
Aqueous dispersion
SAXS
WAXS

ABSTRACT

Oxyethylene (EO) units known from nonionic amphiphiles of the type $C_n(EO)_m$ have been used as a spacer between the hydrophobic and hydrophilic parts of phospholipid molecules. Here we describe the synthesis of the compounds and present results of aqueous dispersions of phospholipids with 3 and 6 EO units. The mechanism of the phase transition from ordered gel to a liquid-crystalline L_α-phase depends on the number of the EO units. In the case of $DH(EO)_3PC$, the lipid head groups are interdigitated in the L_β-phase. On heating, first the head groups de-interdigitate and the melting of the hydrocarbon chains starts only after reaching a stretched head group conformation. While on heating the lamellar repeat distance changes continuously, the cooling process is more complex showing two regimes for the decrease of the lamellar repeat distance. In the case of $DH(EO)_6PC$, the same transition occurs in a single step without any hysteresis between heating and cooling.

1. Introduction

Oxyethylene (EO) units are important hydrophilic head groups of nonionic amphiphiles, which can build adsorption layers at surfaces or can self-aggregate to form micelles or lyotropic mesophases. Their properties are widely used and applications range from fabrication of cosmetic care products and detergents to oil production. In the ternary system water, amphiphile and oil, microemulsions were observed that show a rich variety of phases depending on temperature, composition and length of the hydrophobic chains or the number of EO units [1,2]. These different phases mainly result from the properties of corresponding binary mixtures [3]. Depending on the ratio between the hydrophilic (number of EO units) and hydrophobic (length of the hydrophobic chains) parts, the phase diagram of such mixtures can vary considerably [4,5]. Moreover their thermally induced phase transitions can depend on the rate of temperature changes [6].

Phospholipids are also able to form superstructures when they are dispersed in water. The type and the properties of these structures depend on the chemical characteristics of the single phospholipid molecule. Thereby, the chemical modification of phospholipid molecules opens the possibility to prepare lipid systems with special properties and is an option to change the properties of known lipid systems by the addition of chemically modified lipids. Chemically modified lipids are useful tools, e.g., to study the influence of the chemical structure on the characteristics of membranes and vesicles. They also could be helpful in the preparation of lipid aggregates with improved stability, loading capacity or specificity of action. With respect to biological membrane systems it is of great interest to study how membrane–protein interactions are influenced by structurally modified phospholipids.

EO units have been extensively used as spacers to separate lipid head groups from the hydrophobic part without introducing electrical charges into the system. It has been shown that the number of EO groups modifies significantly the structural behavior of lipid-based model membranes [7–10]. Furthermore such hydrophilic spacers can strongly influence intra- and intermolecular interactions in thin films. They play an important role in coupling mechanisms at surfaces and interfaces. In the system Streptavidin/Biotin the lateral protein density is mainly dependent on the length of the spacer between the biotin and the hydrophobic anchor of the functionalized lipid [11–13].

The introduction of EO units into the hydrophilic head group of phospholipids results in an increase of the main-transition temperature and of the hydration ability of the aqueous lipid dispersions [14]. Lipids with polyethylene glycol (PEG) modified head groups can be used to increase the stability of liposome preparations because they influence the fusion behavior and modify the interactions between plasma proteins and liposomal systems [15–17]. The hydrophilic head group spacer used should allow a more flexible arrangement of the phosphocholine head groups in aggregated

* Corresponding author. Tel.: +49 (0)331 567 9234; fax: +49 (0)331 567 9202.
E-mail address: brezesinski@mpikg.mpg.de (G. Brezesinski).

0927-7757/$ – see front matter © 2009 Elsevier B.V. All rights reserved.
doi:10.1016/j.colsurfa.2009.10.027

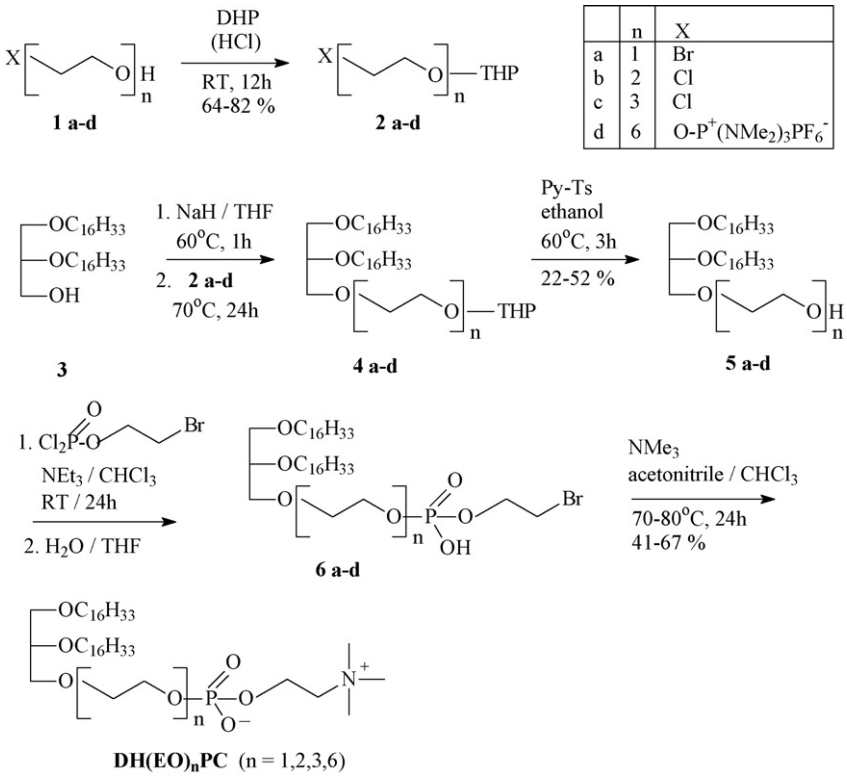

Scheme 1. Synthesis of phosphocholines of the DH(EO)$_n$PC type.

lipid structures. This may cause a change in the physical–chemical properties of the lipid superstructures, especially in the case of lipid mixtures. Membranes containing these lipids may also exhibit a differing behavior towards surface active enzymes (e.g., phospholipases) or other proteins and biologically relevant compounds [15–17].

In this work, the synthesis of racemic phospholipids with hydrophilic spacers (EO units) between the lipophilic part of the molecule (dialkylglycerol) and the phosphocholine head group (DH(EO)$_n$PCs, Scheme 1) as well as the phase behavior of two phospholipids with 3 and 6 EO units as a function of temperature in aqueous dispersions are described. The properties of the different phases and the mechanisms of phase transitions will be discussed in detail in terms of inter- and intramolecular interactions and geometric packing constraints.

2. Materials and methods

The ethylene glycol monochlorohydrines were purchased from Fluka, bromoethanol was from Aldrich and the rac-1,2-di-O-hexadecylglycerol was from Bachem. The silica gel and the solvents were Merck products.

The FAB-MS was made at an AMD 402 (AMD Intectra GmbH, Bremen) with thioglycerol as matrix. The ^{1}H NMR-spectra were recorded using a Gemini 200 (Varian) at 27 °C in $CDCl_3$.

The lipids investigated were 11-hexadecyloxy-3,6,9,13-tetraoxanonacosyl-phosphocholine (DH(EO)$_3$PC) and 20-hexadecyloxy-3,6,9,12,15,18,22-heptaoxa-octatriacontyl-phosphocholine (DH(EO)$_6$PC). Weighed amounts of lipids (20% w:w) were dispersed in ultra-pure water (specific resistance > 18 MΩ cm), incubated above the corresponding main-transition temperature and vortexed for 5 min. The dispersions were filled into X-ray capillaries of 1 mm diameter (Hilgenberg, Germany) and stored at 4 °C for at least 24 h.

Time-resolved diffraction experiments were performed at the X13 double focusing monochromator-mirror camera of the EMBL outstation at DESY in Hamburg using Synchrotron X-ray radiation from the storage ring DORIS III. The wavelength was fixed to 0.15 nm. The diffracted intensities in the small- (SAXS) and wide-angle (WAXS) regions were simultaneously recorded by two linear delay-line detectors [18] connected in series. The data acquisition system has been described elsewhere [19–21]. Diffraction patterns were recorded during heating and cooling with a scan rate of 1.5 K/min. The sample temperature was adjusted by a temperature controlled water bath. To minimize the X-ray dose on the sample, a fast selenoid driven shutter was used. In the experiments, an alternating sequence of 30 s exposure time and 30 s waiting time was used. The reciprocal spacings $s = 1/d$ were calibrated with the diffraction pattern of dry rat-tail collagen which has a long spacing of 65 nm (SAXS) and p-bromo-benzoic acid (WAXS).

3. Results

3.1. Synthesis of the DH(EO)$_n$PCs (Scheme 1)

The DH(EO)$_n$PC lipids with $n = 1$–3 were prepared by protecting commercially available ethylene glycol monochlorohydrines **1** (bromoethanol in the case of $n = 1$) with dihydropyrane (DHP) and subsequent ether coupling with racemic di-O-hexadecylglycerol **3**. After deprotection with pyridinium tosylate/ethanol [22], the resulting glycerol derivatives **4** were converted into the DH(EO)$_n$PCs by reaction with β-bromoethylphosphoric acid dichloride followed by treatment with triethylamine [23]. The final products were purified by column chromatography. The overall yields range from 14 to 22% starting from 1,2-di-O-hexadecylglycerol **3**. For the preparation of the DH(EO)$_6$PC a monohalogenated hexaethylene glycol was not commercially available. In this case, we prepared the phosphonium salt **1d** according to the procedure of Selve et al. [24] and used it in an

analogous manner as starting material. The purity and identity of the $DH(EO)_nPCs$ were checked by elemental analysis, FAB-MS and ^1H NMR.

Triethylene glycol monochlorohydrine tetrahydropyranylether **2c**: 43.7 ml (0.3 mol) triethylene glycol monochlorohydrine **1c** and three drops of concentrated HCl were mixed. Under stirring with a magnetic stirrer the mixture was cooled to 0 °C and 43 ml (0.5 mol) DHP, freshly distilled over NaOH, were added in small portions. After standing overnight at room temperature the solution was diluted with 250 ml diethylether and neutralized by stirring with 0.15 g powdered NaOH for 30 min. The solids were filtered off and the solvent and excessive DHP were removed under reduced pressure. The reaction product was purified by distillation: Kp. 128–131 °C/0.6 mm. Yield: 54.6 g (72%) $C_{11}H_{21}ClO_4$ (MW: 252.74). Calc.: C 5.28, H 8.38, Cl 14.03; found: C 51.89, H 8.45, Cl 13.66.

Diethyleneglycol monochlorohydrine tetrahydropyranylether **2b**: Preparation as described for compound **2c**. Kp. 69–70 °C/0.1 mm. Yield: 80.4 g (77%) $C_9H_{17}ClO_3$ (MW: 208.69). Calc.: C 51.80, H 8.21, Cl 16.99; found: C 51.64, H 8.11, Cl 17.47.

2-Bromoethyl-tetrahydropyranylether **2a**: Preparation as described for compound **2c**. Kp. 98–100 °C/15 mm. Yield: 81.2 g (78%) $C_7H_{13}BrO_2$ (MW: 209.08). Calc.: C 40.21, H 6.30, Br 38.16; found: C 39.81, H 6.32, Br 37.79.

1-O-(2,3-Di-O-hexadecyloxypropyl)-triethyleneglycol **4c**: 0.45 g NaH (60%, 11 mmol) were suspended in 25 ml dry THF under an argon atmosphere. 5.41 g (10 mmol) rac-1,2-di-O-hexadecylglycerol **3**, dissolved in 25 ml dry THF, was added dropwise at room temperature. After stirring the mixture for 1 h at 50 °C, 0.32 g (10 mol%) NBu_4Br and 4.0 g (15.8 mmol) triethylene glycol monochlorohydrine tetrahydropyranylether **2c**, dissolved in 10 ml dry THF, were dropped into the solution.

The mixture was stirred for 12 h at 50 °C and the conversion was checked by TLC. After cooling to room temperature, 250 ml ether was added. The mixture was filtered and the ether phase was repeatedly washed with water, dried over Na_2SO_4 and the solvents were removed in vacuum. The residue was dissolved in 100 ml ethanol. 330 mg pyridinium tosylate were added and the solution was stirred for 3 h at 60 °C. The ethanol was then removed in vacuum, the crude product was dissolved in ether and washed twice with water. The ether phase was dried (Na_2SO_4), the solvent was evaporated and the product was purified by filtration over a short column of silica gel with heptane/chloroform 1:1 as eluent. Fp. 33–34 °C. Yield: 3.98 g (59%) $C_{41}H_{84}O_6$ (MW: 673.13). Calc.: C 73.16, H 12.58; found: C 73.06, H 12.50. Rf = 0.16 ($CHCl_3$/ether 8:2).

^1H NMR: 0.86 t, 6H ($2CH_3$); 1.24 s, 52H (1,2-di-O-alkyl: $26CH_2$); 1.40–1.62 m, 4H (1,2-di-O-alkyl: $2\underline{CH_2}–CH_2–O$); 2.46 s (b), 1H (OH); 3.34–3.60 m, 11H ($2CH–\underline{CH_2}–O–\underline{CH_2}$; $\underline{CH}–O–\underline{CH_2}$); 3.62–3.64 m, 8H ($4CH_2$; ethoxy units); 3.65–3.75 m 2H ($\underline{CH_2}–OH$).

1-O-(2,3-Di-O-hexadecyloxypropyl)-diethyleneglycol **4b**: Same procedure as described for compound **4c**. Fp. 33–34 °C. Yield: 2.97 g (47%) $C_{39}H_{80}O_5$ (MW: 629.07). Calc.: C 74.46, H 12.82; found: C 74.30, H 12.89. Rf = 0.28 ($CHCl_3$/ether 8:2).

^1H NMR: 0.86 t, 6H ($2CH_3$); 1.24 s, 52H (1,2-di-O-alkyl: $26CH_2$); 1.39–1.60 m, 4H (1,2-di-O-alkyl: $2\underline{CH_2}–CH_2–O$); 2.46 s (b), 1H (OH); 3.36–3.74 m, 17H ($2CH–\underline{CH_2}–O\underline{CH_2}$; $\underline{CH}–O–\underline{CH_2}$; $O–CH_2–\underline{CH_2}–O–\underline{CH_2}–\underline{CH_2}–OH$).

1-O-(2,3-Di-hexadecyloxypropyl)-ethyleneglycol **4a**: Same procedure as described for compound **4c**. Fp. 34–35 °C. Yield: 3.10 g (53%) $C_{37}H_{76}O_4$ (MW: 528.02). Calc.: C 75.97, H 13.09; found: C 75.83, H 13.03. Rf = 0.31 ($CHCl_3$/ether 8:2).

^1H NMR: 0.86 t, 6H ($2CH_3$); 1.23 s, 52H (1,2-di-O-alkyl: $26CH_2$); 1.39–1.60 m, 4H (1,2-di-O-alkyl: $2\underline{CH_2}–CH_2–O$); 2.45 s (b), 1H (OH); 3.37–3.71 m, 13H ($2CH–\underline{CH_2}–O\underline{CH_2}$, $\underline{CH}–O\underline{CH_2}–\underline{CH_2}–OH$).

11-Hexadecyloxy-3,6,9,13-tetraoxanonacosyl-phosphocholine ($DH(EO)_3PC$): To a solution of 1 g (4 mmol) 2-bromoethyl-phosphoric acid dichloride and 0.92 ml (7 mmol) triethylamine in 5 ml abs. chloroform a solution of 1.35 g (2 mmol) 1-O-(1,2-dihexadecyloxypropyl)-triethyleneglycol **4c** in 10 ml abs. chloroform was added dropwise within 1 h under stirring at room temperature. The mixture was stirred for further 24 h and the conversion was checked by TLC. Then 10 ml water and 10 ml THF were added and stirring was continued for 60 min. The mixture was mixed with 10 ml diisopropylether, 100 ml formic acid (2%) and 5 ml methanol. After shaking in a separation funnel the aqueous phase was separated, 10 ml of 1 M Na-acetate solution and 5 ml methanol were added and the mixture was shaken another time. The organic phase was dried over Na_2SO_4 and the solvent was removed under reduced pressure. The crude product was resolved in 5 ml dry chloroform and mixed with 4 ml of a solution of trimethylamine in acetonitrile (30% = 20 mmol trimethylamine). The mixture was sealed in a round bottom flask and heated for 2 days at 60 °C. After removing the solvent the product was purified by chromatography in the following manner: 60 g silica gel per gram crude product; subsequent elution with (1) $CHCl_3/CH_3OH$ 8:2, 500 ml; (2) $CHCl_3/CH_3OH/NH_3$ (25%) 80:20:2, 1000 ml; (3) $CHCl_3/CH_3OH/NH_3$ (25%) 65:35:5 until the final product was completely eluted. Yield: 634 mg (37%) $C_{46}H_{96}NO_9P·H_2O$ (MW: 856.27). Calc.: $P = 3.62$; found: $P = 3.57$. Rf = 0.20 [$CHCl_3/CH_3OH/NH_3$ (25%) 66:35:5]. FAB-MS: Calc.: $M = 838.25$; found: 839 ($M+H^+$).

^1H NMR: 0.86 t, 6H ($2CH_3$); 1.23 s, 52H (1,2-di-O-alkyl: $26CH_2$); 1.52 m, 4H (1,2-di-O-alkyl: $\underline{CH_2}–CH_2–O$); 3.34 s 9H ($N^+[CH_3]_3$); 3.36–3.56 m, 9H (glycerol: $\underline{CH_2}–\underline{CH}–\underline{CH_2}$; 1,2-di-O-alkyl: $2CH_2–\underline{CH_2}–O$); 3.59 s, 10H (ethoxy units: $\underline{CH_2}–\underline{CH_2}–O–\underline{CH_2}–\underline{CH_2}–O\underline{CH_2}CH_2OP$); 3.80 m, 2H ($CH_2–N^+$); 4.31 m, 2H ($\underline{CH_2}OP$).

8-Hexadecyloxy-3,6,10-trioxahexacosyl-phosphocholine ($DH(EO)_2PC$): Yield: 666 mg (41%) $C_{44}H_{92}NO_8P·H_2O$ (MW: 812.22). Calc.: $P = 3.81$; found: $P = 3.74$. Rf = 0.21 ($CHCl_3/CH_3OH/NH_3$ (25%) 66:35:5). FAB-MS: Calc.: $M = 794.20$; found: 794 (M^+).

^1H NMR: 0.85 t, 6H ($2CH_3$); 1.23 s, 52H (1,2-di-O-alkyl: $26CH_2$); 1.52 m, 4H (1,2-di-O-alkyl: $\underline{CH_2}–CH_2–O$); 3.32 s 9H ($N^+[CH_3]_3$); 3.35–3.55 m, 9H (glycerol: $\underline{CH_2}–\underline{CH}–\underline{CH_2}$; 1,2-di-O-alkyl: $2CH_2–\underline{CH_2}–O$); 3.57 m, 6H ($\underline{CH_2}–\underline{CH_2}–O\underline{CH_2}–\underline{CH_2}OP$); 3.78 m, 2H ($\underline{CH_2}–N^+$); 3.92 m, 2H ($CH_2–CH_2–N^+$); 4.28 m, 2H ($\underline{CH_2}–OP$).

5-Hexadecyloxy-3,7-dioxatricosyl-phosphocholine ($DH(EO)_1PC$): Yield: 490 mg (32%) $C_{42}H_{88}NO_7P·H_2O$ (MW: 768.17). Calc.: $P = 4.03$; found: $P = 4.11$. Rf = 0.21 ($CHCl_3/CH_3OH/NH_3$ (25%) 65:35:5). FAB-MS: Calc.: $M = 750.15$; found: 750 (M^+).

^1H NMR: 0.85 t, 6H ($2CH_3$); 1.23 s, 52H (1,2-di-O-alkyl: $26CH_2$); 1.51 m, 4H (1,2-di-O-alkyl: $\underline{CH_2}–CH_2–O$); 3.31 s 9H ($N^+(CH_3)_3$); 3.36–3.55 m, 9H (glycerol: $\underline{CH_2}–\underline{CH}–\underline{CH_2}$; 1,2-di-O-alkyl: $2CH_2–\underline{CH_2}–O$); 3.60 m, 2H ($O–\underline{CH_2}–\underline{CH_2}–OP$); 3.75 m, 2H ($CH_2–N^+$); 3.93 m, 2H ($\underline{CH_2}–CH_2–N^+$); 4.28 m, 2H ($\underline{CH_2}–OP$).

Synthesis of hexaethyleneglycol-monooxy-tris-(dimethylamino)-phosphonium hexafluoro-phosphate **1d**: The synthesis was performed according to Selve et al. [24].

Preparation of **2d** (tetrahydropyranylation of **1d**): The oily product **1d** was dissolved in 80 ml chloroform and 6.29 g (6.8 ml; 0.075 mol) DHP (freshly distilled over NaOH) and 1.26 g (5 mmol) pyridinium tosylate were added. The mixture was stirred overnight at room temperature, then filtered and evaporated in vacuum. The crude product **2d** was used without further purification.

Synthesis of rac.-1-O [2′3′-di-O-hexadecyloxypropyl-]hexaethylene glycol **4d**: 2.7 g 1,2-di-O-hexadecylglycerol **3** (5 mmol) were dissolved in 50 ml dry THF and 240 mg NaH (60%; 6 mmol) were added. The mixture was stirred under argon at room temperature for 15 min and then heated at 60 °C for 1 h. Then 3.4 g **2d** (5 mmol) were added and the solution was stirred at 60 °C for 24 h. After cooling to room temperature, 1 ml water was added while stirring the mixture followed by addition of 100 ml ether. The organic layer was washed with water until the aqueous phase was neutral. After drying over Na_2SO_4 and evaporation in vacuum, the residue was dissolved in 50 ml ethanol and 0.2 g pyridinium tosylate (0.8 mmol) were added. The solution was heated at 60 °C for 3 h (TLC-control). The mixture was filtered, evaporated in vacuum and purified on a silica gel column with toluene/acetone (9:1) as eluent. Yield: 1.75 g (43.5%) $C_{47}H_{96}O_9{\cdot}H_2O$ (MG: 823.28). Calc.: C 68.47%, H 12.00%; found: C 68.39%, H 11.87%. Rf = 0.05 ($CHCl_3$/ether 8:2), Fp. 32–34 °C.

^{1}H NMR: 0.86 t, 6H ($2CH_3$); 1.24 s, 52H (1,2-di-O-alkyl: $26CH_2$); 1.53 m, 4H (1,2-di-O-alkyl: $2\underline{CH_2}–CH_2–O$); 2.51 t 1H (OH); 3.38–3.58 m, 9H (1,2-di-O-alkyl glycerol: $\underline{CH_2}–O\underline{CH}$–alkyl; CH–O–$\underline{CH_2}$ alkyl$\underline{CH_2}$–O = glycerol C3); 3.60–3.66 m, 22H [O–($\underline{CH_2}–\underline{CH_2}$)$_5$–$\underline{CH_2}CH_2OH$]·3.71 m, 2H ($\underline{CH_2}$–OH).

20-Hexadecyloxy-3,6,9,12,15,18,22-heptaoxa-octatriacontyl-phosphocholine (DH(EO)$_6$PC): 805 mg **4d** were dissolved in 15 ml of dry toluene and 0.16 ml triethylamine (1.14 mmol) were added. The solution was cooled to 0 °C and mixed with 0.11 g (0.1 ml) 2-chloro-2-oxo-1,3,2-dioxaphospholane (1 mmol). The mixture was stirred under argon overnight at room temperature and then filtered and evaporated in vacuum. The crude intermediate was dissolved in 20 ml of dry butanone. After addition of 0.18 g LiBr (1 mmol) the mixture was refluxed for 6 h, evaporated in vacuum and resolved in chloroform. The chloroform solution was filtered and evaporated to a volume of 10–20 ml. Then 10 ml of trimethylamine (50% solution in acetonitrile) were added. The occurring turbidity was resolved by dropwise addition of chloroform. The mixture was stirred at 60 °C for 48 h and then evaporated. The crude product was purified by chromatography on silica gel with chloroform/methanol/NH_3 (25%) 80:20:2. Yield: 176 mg (18.2%) $C_{52}H_{108}NO_{12}P{\cdot}H_2O$ (MG: 988.41). Calc.: P = 3.13; found: 2.98. FAB-MS: $C_{52}H_{108}NO_{12}P$, molpeak: Calc.: 970.39; found: 971 ($M+H^+$).

^{1}H NMR: 0.85 s, 6H ($2CH_3$); 1.23 s, 52H (1,2-di-O-alkyl: $26CH_2$); 1.52 m, 4H (1,2-di-O-alkyl: $2\underline{CH_2}–CH_2–O$); 3.35 s 9H (N $(CH_3)_3$); 3.35–3.56 m, 9H (glycerol: $\underline{CH_2}–\underline{CH}–\underline{CH_2}$ 1,2-di-O-alkyl; $2CH_2–\underline{CH_2}–O$); 3.60 s, 22H (($\underline{CH_2}–\underline{CH_2}O)_5$–$\underline{CH_2}CH_2OP$)·3.82 m, 2H ($\underline{CH_2}$–N); 3.98 m, 2H ($\underline{CH_2}–CH_2–N$); 4.33 m, 2H ($\underline{CH_2}OP$).

3.2. DH(EO)$_3$PC

The sample was several times heated and cooled between 5 °C and 95 °C. This procedure is convenient because it allows phase sequence identification, determination of phase transition temperatures and observation of a possible hysteresis. Fig. 1 shows the time-resolved diffraction patterns recorded during heating. At low temperature, three diffraction peaks are observed in the SAXS region with reciprocal spacings in a ratio of 1:2:3, indicating a lamellar phase. During heating, the repeat distance increases slightly from 6.23 nm at 6 °C to 6.55 nm at 37 °C (Fig. 2). Only one sharp peak can be seen in the WAXS region. This leads to the assumption of hexagonal packing of untilted chains in an all-trans conformation (L_β-phase). The reciprocal spacing (s) of the chain lattice slightly decreases on going from 6 °C to 37 °C (Fig. 3, indicated by the detector channel position of the Bragg peak maximum). Therefore, the corresponding cross-sectional area per chain increases from 0.194 nm^2 to 0.196 nm^2 in this temperature interval. At the same time, the integral intensity of the WAXS Bragg peak continuously increases. Interestingly, the maximum intensity of the peak increases till ~32 °C, and then it decreases slightly until the transition into the L_α-phase. Above 37 °C, the third order peak in the SAXS region vanishes and a strong continuous shift of the remaining two peaks towards smaller s values (larger d-spacings) is observed. This shift is completed at 44.5 °C with a lamellar spacing of 8.6 nm. The two dashed lines mark this transition region in Fig. 2. The diffraction patterns in the WAXS region still indicate order in the chain lattice. Only above 45 °C, the melting of the aliphatic chains occurs, indicated by the disappearance of the sharp reflec-

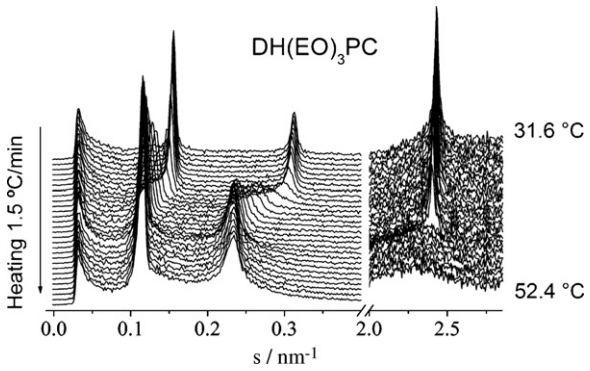

Fig. 1. First heating sequence of scattering patterns (scattering intensity vs. s) of the DH(EO)$_3$PC/water system, showing the shift of the peak positions during the phase transition from L_β- to L_α-phase. The starting and final temperatures of this scan are indicated. The completion of the phase transition can be recognized by the sudden disappearance of the peak in the WAXS region. The chain packing is hexagonal.

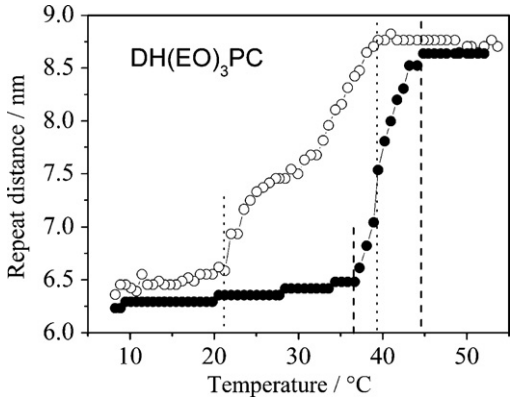

Fig. 2. The variation of the interplanar repeat distance with temperature during heating (●) (scan shown in Fig. 1) and cooling (○). The phase transition on heating spans over about 7 K and is a continuous process. However, the phase transition upon cooling is a multiple process that spans over a much wider temperature range, despite a hysteresis of ca. 4 K. Note that the change in d-spacing is significantly large. The dashed lines mark the de-interdigitation of the head groups during heating, and the dotted lines show the temperature interval in which the head groups interdigitate during cooling.

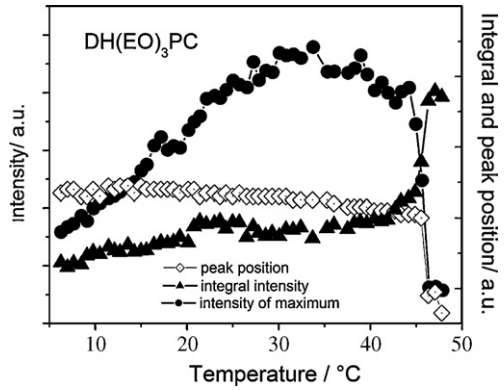

Fig. 3. Maximum (●) and integral (▲) intensities of the WAXS peak and the respective peak positions (as detector channel) (◊) versus temperature. The shift towards lower channels indicates an expansion of the hexagonal lattice. Note that the maximum intensity increases until 32 °C, indicating a continuous improvement of the chain packing, but this is not connected with significant changes in the position or integral intensity.

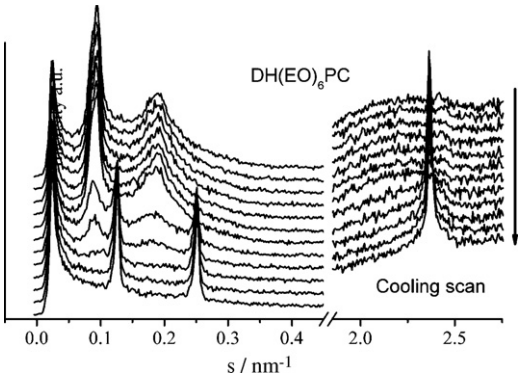

Fig. 5. Cooling sequence of scattering patterns (scattering intensity vs. *s*) of the $DH(EO)_6PC$/water system, showing the shift of the peak positions during the phase transition from L_α to L_β. The transition is connected with a coexistence of two phases. The FWHM of the Bragg peaks are very different in the two phases indicating different correlation lengths between the bilayers. The chain packing in the gel phase is hexagonal.

tion in the WAXS, which is replaced by a broad halo. The melting transition is not connected with any further change in the position of the SAXS peaks. The repeating distance remains practically constant. This melting transition can only be visualized by the evolution of the WAXS patterns (Figs. 1 and 3). These data can be interpreted in the following way: heating causes increasing thermal vibrations, responsible for the small increase in the separation between coplanar chains. Simultaneously, the intermolecular order increases, seen by a sharpening of the WAXS peak. The FWHM decreases continuously up to 25 °C when it becomes constant until the phase transition temperature is reached (Fig. 4). One can speculate that up to 25 °C there is a continuous long-range ordering. Till 32 °C, an additional improvement of the packing can be seen by the increase of the peak intensity. In this case the ordering seems to be more localized, improving at short distance an already existing hexagonal lattice of alkyl chains. Therefore, the WAXS peak becomes more intense but not sharper. This would reflect an increasing contribution of molecules placed in a well-organized lattice, which should contain the smallest number of defects in the layers. Above 32 °C up to the phase transition, the decrease of the peak intensity, despite maintaining the same FWHM, could be attributed to a decrease in the number of molecules contributing to this well-organized lattice. This intuitively suggests that the melting process starts at the borders of the gel crystallites, moving towards the centre as the temperature raises [25].

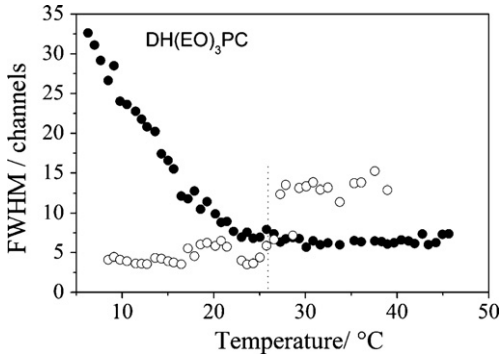

Fig. 4. The FWHM of the WAXS peak upon heating (●) and cooling (○) from 95 °C. Upon heating, it decreases continuously until ca. 25 °C (the dotted line is only to guide the eye) and then remains constant until the phase transition. On cooling, the smaller FWHM at lower temperatures indicates a far better packing of the molecules compared with the initially observed one.

On cooling the sample from 95 °C, one observes at the onset of the gel phase a FWHM larger than that observed on heating (Fig. 4). However, upon reaching 25 °C it decreases suddenly. This decrease in FWHM of the WAXS peak seems to be connected with the second step in the decrease of the interlamellar distance.

The phase transition from the L_α- to the L_β-phase is reversible but shows a pronounced hysteresis of about 5 K at the onset of the phase transition. Additional to this hysteresis, the heating and cooling paths show appreciable differences (see Fig. 2). While on heating the lamellar repeat distance changes continuously, the cooling is more complex showing two regimes for the decrease of the lamellar repeat distance. On cooling, the *d*-spacing first decreases similar to the observed increase during heating. Between 32 °C and 25 °C, the decrease in the bilayer thickness is much slower, almost characterized by a plateau region. Then, an additional linear decrease can be seen. The changes are completed at 21 °C, showing that the hysteresis amounts to approximately 15 K at the end of the transition. This was taken as evidence for a phase transition mechanism involving two successive processes during cooling. Our data do not allow identification or characterization of possible meta-stable phases. Again, the wide-angle contribution for the scattering pattern is used to obtain further insight into the phase transition process. The chains pack again in a hexagonal lattice seen by the appearance of a sharp WAXS peak. On cooling the sample, this peak shifts continuously towards smaller *d*-values and increases its intensity (until ca. 25 °C, data not shown). Similar to the heating scan, the transition from the liquid-like (α) state of the hydrocarbon chains to the gel (β) state is not connected with the change in the bilayer thickness. The chains are already in an ordered state before the decrease of the *d*-value starts. At 40 °C, the cross-sectional area in the gel phase amounts to 0.202 nm^2 and decreases continuously to 0.195 nm^2 at 27 °C. A second heating cycle leads again to an increase of the lamellar distance from 6.6 nm to 8.6 nm between 36 °C and 44 °C. The hexagonal packing of the alkyl chains persists up to 45 °C with an area per chain of 0.200 nm^2. The phase transition from the gel to the L_α-phase occurs between 45.5 °C and 46.2 °C. This shows again that the chain melting occurs only after the drastic increase of the lamellar spacing is completed.

3.3. $DH(EO)_6PC$

At lower temperatures, the phospholipid with a hydrophilic spacer of 6 EO units shows two Bragg peaks in the SAXS and one sharp reflection in the WAXS (Fig. 5). The ratio of the positions

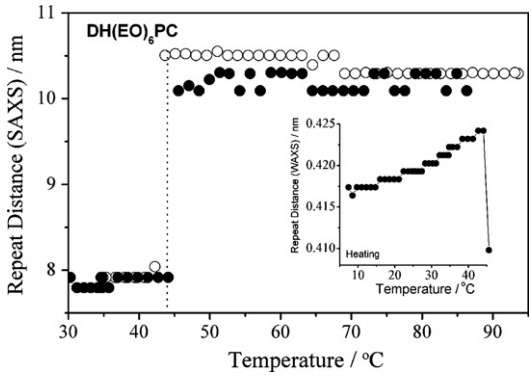

Fig. 6. Interplanar repeat distance versus temperature during heating (●) and cooling (○) (scans shown in Fig. 5). Despite heating and cooling rates of 1.5 K/min, the phase transition shows no hysteresis and is a single (jump) process. The inset shows the *d*-values determined from the WAXS region. The cross-sectional area of the chains increases continuously until the melting process.

of the first and second order reflections in the small-angle region indicates a lamellar L_β-phase. At a temperature of 7 °C a lamellar distance of 7.81 nm is observed. The sharp diffraction peak in the WAXS indicates hexagonal symmetry of the chain lattice. The spacing of 0.417 nm gives a cross-sectional area per chain of 0.201 nm^2. On heating the sample to 42.7 °C, the lamellar distance increases slightly to 7.91 nm and the cross-sectional area increases continuously to 0.208 nm^2 (inset of Fig. 6). Between 42.7 °C and 44.6 °C, the coexistence of two phases with very different lamellar spacings can be observed (Fig. 5). The intensity of the sharp reflection in the wide-angle region decreases continuously with increasing temperature. At 45 °C, this reflection disappears completely and the broad halo shows that the chains are molten. The lamellar distance of the L_α-phase is increased to 10.25 nm. Further heating leads to a slight decrease of the lamellar distance. On cooling the sample, an expansion of the bilayer distance to 10.7 nm at 43.7 °C was observed. Between 43.7 °C and 39.4 °C, there is again coexistence between L_α and L_β. The reflection in the wide-angle region corresponds to a hexagonal packing of upright oriented chains. At the end of the transition (39.4 °C), the lamellar spacing decreased to 7.91 nm (Fig. 6). On further cooling, the lamellar distance changes only slightly and the chain lattice is unchanged. In a second heating cycle, the two-phase region of the gel- and the L_α-phase can be seen between 42.5 °C and 44.5 °C. A second cooling cycle confirmed the complete reproducibility of this phase sequence. In contrast to $DH(EO)_3PC$, the melting of the hydrocarbon chains and the drastic increase of the bilayer thickness are directly connected.

4. Discussion

The molecular lengths of $DH(EO)_3PC$ and of $DH(EO)_6PC$ were calculated for different states using a MM2 force field [26]. According to the observed WAXS diffraction patterns, an upright orientation of the hexagonally packed hydrophobic chains within the bilayers can be assumed. Therefore, the contribution of the C_{16} chains in all-trans conformation to the bilayer thickness is approximately 2×2.04 nm (15×0.126 nm + 0.15 nm) = 4.08 nm [27]. The molecular spacing strongly depends on the conformation of the EO-spacer and the head group, as well as on the thickness of the water layer between the lipid bilayers. In the case of $DH(EO)_3PC$, a thickness of only 2.1–2.5 nm (depending on the temperature) is left for the glycerol backbone, the spacer, the head group and the water layer. Assuming an extended conformation for all of the hydrophilic parts (head group and EO-spacer) of the molecule, one gets approximately 2.2 nm for one monolayer in the bilayer. The cross-sectional chain area and the hexagonal packing of upright oriented chains lead to a molecular area of only 0.40 nm^2. This value is much smaller than observed in double-chain phosphatidylcholines both in bilayers and monolayers [28–31]. Usually the PC head group requires a molecular area of 0.45 nm^2 and forces the chains into a tilted conformation to optimize their van der Waals interactions. Therefore, for the phosphatidylcholines with EO-spacers one has to assume a different head group conformation leading to a smaller molecular area. The extended head group conformation seems to be the most reasonable one. A tangling of the hydrophilic spacer (meander conformation) reduces the length of the hydrophilic part to 1.9 nm. Such values fit well with the experimentally observed ones if one assumes interdigitation of the hydrophilic head groups. The observed increase in the repeat distance, which starts at 37 °C, seems to indicate that the interdigitated head groups begin to disconnect. At the end of this temperature interval (at 44.5 °C), the lamellar spacing amounts to 8.6 nm. At this stage, the observed difference in the bilayer thickness is only a result of the changed head group conformation and the water layer because the hydrocarbon chains are still in an all-trans conformation and upright. The difference in the *d*-values is approximately 2.1 nm and can be easily explained by extended head group and spacer conformations with a small contribution of a water layer between the now oppositely arranged head groups. The calculated lamellar distance of 8.5 nm assuming a stretched conformation of the head group and hydrophilic spacer fits the measured distance of 8.6 nm very well. The melting of the hydrocarbon chains starts only after reaching this head group conformation. Therefore, the melting temperature is very similar to the main-transition temperature of the ether lipid DHPC without any EO-spacer [32]. The melting itself leads to a shortening of the hydrophobic part of the molecule. Since the *d*-spacing does not change at this transition, an event increasing the bilayer thickness by the same amount has to be taken into consideration. The only plausible mechanism can be an increase in the water core between the bilayers. On going to higher temperatures, the lamellar distance decreases slightly, typical for molten chains. The transition from the L_α- to the gel-state is more complex. First, the chains go back to the non-tilted all-trans conformation. This reduces the area requirement of the hydrophobic part of the molecule and leads to the interdigitation of the hydrophilic parts. This interdigitation is at least a two-step process. In the first step, the *d*-spacing is reduced by approximately 1.2 nm and in the second one by additional 1 nm.

In the case of $DH(EO)_6PC$, the lipid with 6 EO units as a hydrophilic spacer, the mechanism during the transition is completely different compared with that of $DH(EO)_3PC$. In the L_β-phase, the measured thickness amounts to 7.8–7.9 nm. The WAXS patterns point again to an upright orientation of hexagonally packed hydrophobic chains within the bilayers. Therefore, the contribution of the C_{16} chains in all-trans conformation to the bilayer thickness in the L_β-phase is, as in the case of $DH(EO)_3PC$, approximately 4.08 nm. Therefore, a thickness of 3.8 nm is left for the hydrophilic part of the bilayer and the water layer between the bilayers. This is much more than in the case of $DH(EO)_3PC$ and cannot be explained purely with the longer spacer length. Therefore, we believe that the hydrophilic head groups are not interdigitated. An extended head group conformation needs at least 3.2 nm leading to 6.4 nm for the hydrophilic part of the bilayer without taking into account any water layer. The meander conformation of the hydrophilic spacer reduces whose length to 1.25 nm [33]. Such a meander conformation seems to be the only reasonable one comparing the *d*-values in the gel phase with the calculated length of the molecule. The PC head group has to be tilted to fill on one hand the space above the EO meander and on the other hand to contribute not too much to the length of the molecule. Even a thin

water layer can be included into such a model. The phase transition into the L_α-phase is connected with the chain melting reducing the hydrophobic core to approximately 3.3 nm und the transition of the EO-spacer from the meander to the extended conformation. The calculated lamellar spacing for $DH(EO)_6PC$ with completely expanded spacer and head group amounts to 9.7 nm. The measured lamellar distance of 10.8 nm in the L_α-phase fits the model well assuming an interbilayer water layer of about 1 nm. Above the phase transition, the typical slight decrease of the lamellar distance can be observed with increasing temperature. Additionally, a clearly pronounced two-phase region was observed during heating and cooling of $DH(EO)_6PC$. This means that the melting of the chains and the stretching of the spacer are two events occurring at the same time.

5. Conclusion

Introducing a hydrophilic spacer between the head group and the glycerol backbone of a 1,2-dihexadecylphosphatidylcholine leads to a completely different phase behavior and phase transition mechanism as presented for the corresponding lipid without such a spacer [32]. Furthermore, it could be shown, that the length of the hydrophilic spacer is responsible for the mechanism of the phase transition from the L_β- to the L_α-phase and vice versa. The short EO-spacer in $DH(EO)_3PC$ leads to an interdigitation of the hydrophilic head groups, whereas the longer EO-spacer in $DH(EO)_6PC$ is in a meander conformation in the gel phase and stretches during the transition into the liquid-crystalline L_α-phase. In both cases, the lamellar distance increases. The phase states after the stretching are the same for both systems, but the mechanisms how the stretching and therefore the phase transitions occur as well as the gel-phase structures are completely different and depend on the number of EO units in the hydrophilic spacer.

Acknowledgement

We thank Frank Richter for the program used to calculate the peak parameters in our data sets.

References

[1] M. Kahlweit, R. Strey, Angew. Chem. 97 (1985) 655–669.
[2] M. Kahlweit, R. Strey, G. Busse, J. Phys. Chem. 94 (1990) 3881–3894.
[3] R. Strey, R. Schomaecker, D. Roux, F. Nallet, U. Olsson, J. Chem. Soc., Faraday 86 (1990) 2253–2261.
[4] S.S. Funari, M.C. Holmes, G.J.T. Tiddy, J. Phys. Chem. 96 (1992) 11029–11038.
[5] S.S. Funari, M.C. Holmes, G.J.T. Tiddy, J. Phys. Chem. 98 (1994) 3015–3023.
[6] S.S. Funari, G. Rapp, Proc. Natl. Acad. Sci. 96 (1999) 7756–7759.
[7] S.S. Funari, Eur. Biophys. J. 27 (1998) 590–594.
[8] S.S. Funari, C. di Vita, G. Rapp, Acta Phys. Pol. A 91 (1997) 953–960.
[9] B. Mädler, G. Klose, A. Möps, W. Richter, C. Tschierske, Chem. Phys. Lipids 71 (1994) 1–12.
[10] S.S. Funari, B. Nuscher, G. Rapp, K. Beyer, Proc. Natl. Acad. Sci. 98 (2001) 8938–8943.
[11] M. Ahlers, R. Blankenburg, H. Haas, D. Möbius, H. Möhwald, W. Müller, H. Ringsdorf, H.-U. Siegmund, Adv. Mater. 3 (1991) 39–46.
[12] R. Blankenburg, P. Meller, H. Ringsdorf, C. Salesse, Biochemistry 28 (1989) 8214–8221.
[13] H. Haas, G. Brezesinski, H. Möhwald, Biophys. J. 68 (1995) 312–314.
[14] B. Rattay, W. Rettig, Pharmazie 52 (1997) 679–1679.
[15] D.D. Lasic, Ang. Chem. Int. Ed. Engl. 33 (1994) 1685–1698.
[16] J.K.P. Hoyrup, T.B. Pedersen, O.G. Mouritsen, Cell. Mol. Biol. Lett. 6 (2001) 255–263.
[17] S. Simões, J. Nuno Moreira, C. Fonseca, N. Düzgüne, M.C. Pedroso de Lima, Adv. Drug Del. Rev. 56 (2004) 947–965.
[18] A. Gabriel, Rev. Sci. Instrum. 48 (1977) 1303–1305.
[19] G. Rapp, A. Gabriel, M. Dosiere, M.H.J. Koch, Nucl. Instrum. Methods Phys. Res. A 357 (1995) 178–182.
[20] M.H.J. Koch, J. Bordas, Nucl. Instrum. Methods Phys. Res. A 208 (1983) 461–469.
[21] C. Boulin, R. Kempf, A. Gabriel, M.H.J. Koch, Nucl. Instrum. Methods Phys. Res. A 269 (1988) 312–320.
[22] M. Miyashita, A. Yoshikoshi, P.A. Grieco, J. Org. Chem. 42 (1977) 3772–3774.
[23] H. Eibl, A. Niksch, Chem. Phys. Lipids 22 (1978) 1–8.
[24] C. Selve, B. Castro, P. Leempoel, G. Mathis, T. Gartiser, J.-J. Delpuech, Tetrahedron 39 (1983) 1313–1316.
[25] M. Rappolt, G. Rapp, Ber. Bunsenges. Phys. Chem. 100 (1996) 1153–1162.
[26] N.L. Allinger, J. Am. Chem. Soc. 99 (1977) 8127–8134.
[27] G. Brezesinski, D. Vollhardt, K. Iimura, H. Cölfen, J. Phys. Chem. C 112 (2008) 15777–15783.
[28] J.M. Seddon, R.H. Templer, Handbook of Biological Physics, vol. 1, Elsevier Science B.V., 1995, pp. 97–160.
[29] G. Brezesinski, A. Dietrich, B. Struth, C. Böhm, W.G. Bouwman, K. Kjaer, H. Möhwald, Chem. Phys. Lipids 76 (1995) 145–157.
[30] F. Bringezu, G. Rapp, B. Dobner, P. Nuhn, G. Brezesinski, J. Phys. Chem. B 105 (2001) 1901–1907.
[31] T.J. McIntosh, Biophys. J. 29 (1980) 237–246.
[32] P. Laggner, K. Lohner, G. Degovics, K. Müller, A. Schuster, Chem. Phys. Lipids 44 (1987) 31–60.
[33] M. Rösch, Fette Seifen Anstrichmittel 59 (1957) 745–747.